Supplementary Information:

Polyurethane Microgel based Microtissue: Interface-guided Assembly and Spreading

Michael J. Hill[1], Debanjan Sarkar[1,2,*]

[1]Department of Biomedical Engineering, University at Buffalo, The State University of New York, Buffalo, NY 14260, USA

[2]Department of Chemical and Biological Engineering, University at Buffalo, The State University of New York, Buffalo, NY 14260, USA

*Corresponding author: D. Sarkar
Ph: 716-645-8497, Fax: 716-645-2207
Email: debanjan@buffalo.edu

Supplementary Materials and Methods:

Compucell3D Simulations:

For ECs temperature (T) is set to 50.[1] Parameters for cell type were matched as closely as possible to existing literature including volume (V) and stiffness (λ_{vol}). In particular, for ECs chemotaxis (VEGF), length constraint, and global connectivity plugins were used to ensure proper morphological features and cell behavior. For the chemotaxis plugin, the Lagrange multiplier was reduced relative to suggested values (50 vs. 5000), as it was found to otherwise dominate contact relations between cells and particles. This can be rationalized on the basis of the microtissues being placed within the bulk model protein phases where VEGF diffusion would be reduced. Parameters for MCF-7 were matched with literature values. [2, 3] Because cancer cells display increased motility, a higher T was used. A proliferation plugin was used due to the faster replication rate of cancer cells. Volume of particles was adjusted to have the same relative order as DLS measurements. Contact energies were obtained from calculated energy minimums between each interacting phase in units of kT. This allowed quantitative testing of DLVO and XDLVO theories applied to this system, as previous simulations often use arbitrary contact energy values along with experimentally obtained chemotaxis or cell-shape parameters. ImageJ (NIH) Fraclac software was also used to characterize the fractal dimension (D_f values) of manually traced borders of the aggregates. Similar characterization of Cellular Potts aggregate simulation borders has been done previously with tumor models.[4]

EQ. S1

$$H = \sum_{\vec{i},\vec{j}} J(\tau(\sigma_{\vec{i}}), \tau(\sigma_{\vec{j}}))\left(1 - \delta(\sigma_{\vec{i}}, \sigma_{\vec{j}})\right) + \sum_{\sigma} [\lambda_{vol}(\sigma)\,(v(\sigma) - V_t(\sigma))^2]$$

Supplementary Figures S1-S8:

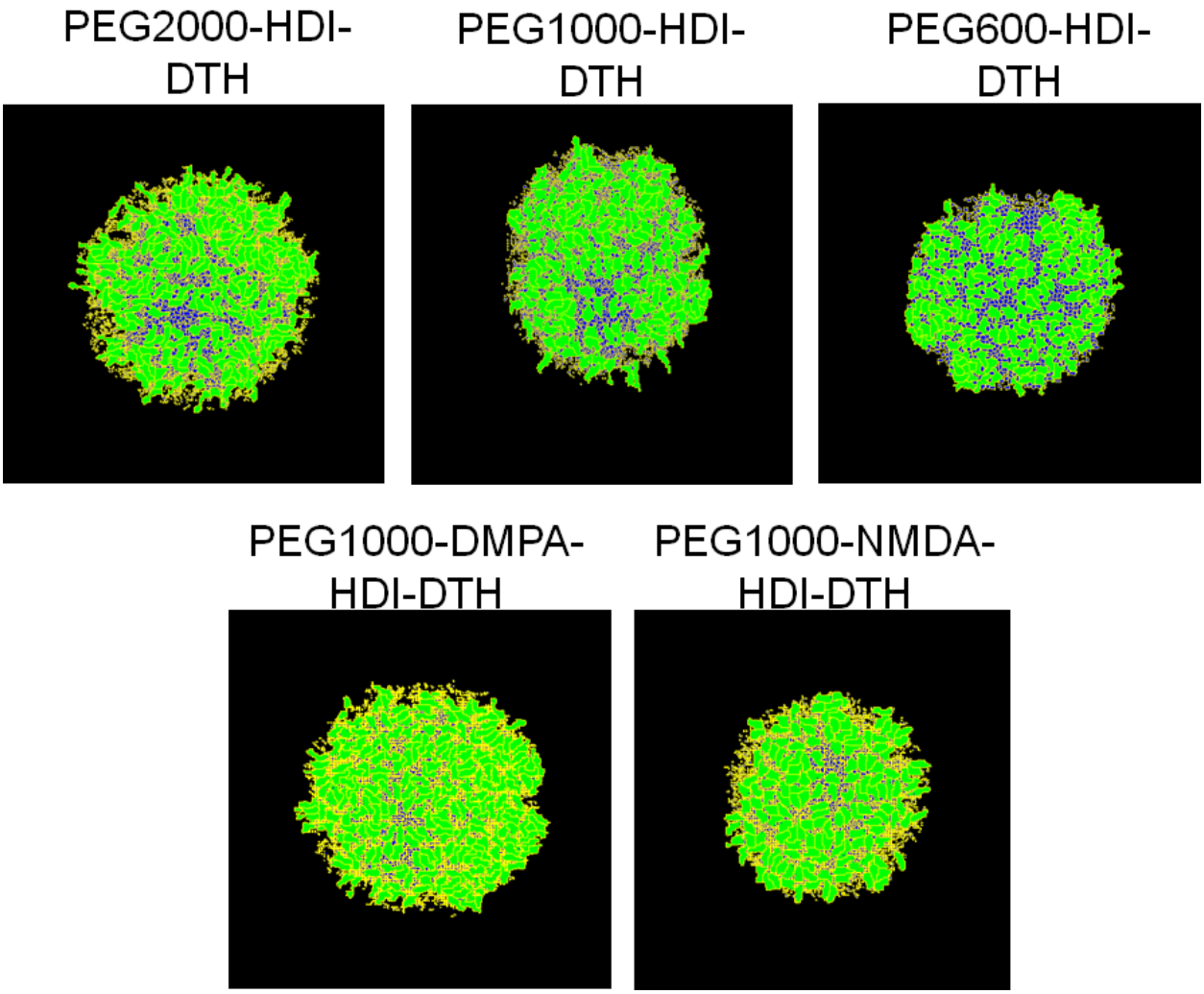

Figure S1: Microtissue Spreading Simulations at Zero Hour Time Point: at the zero hour time point, both cell type microtissues appear similar. Blue or yellowish smaller particles are the microgel particles and larger green objects are the cells.

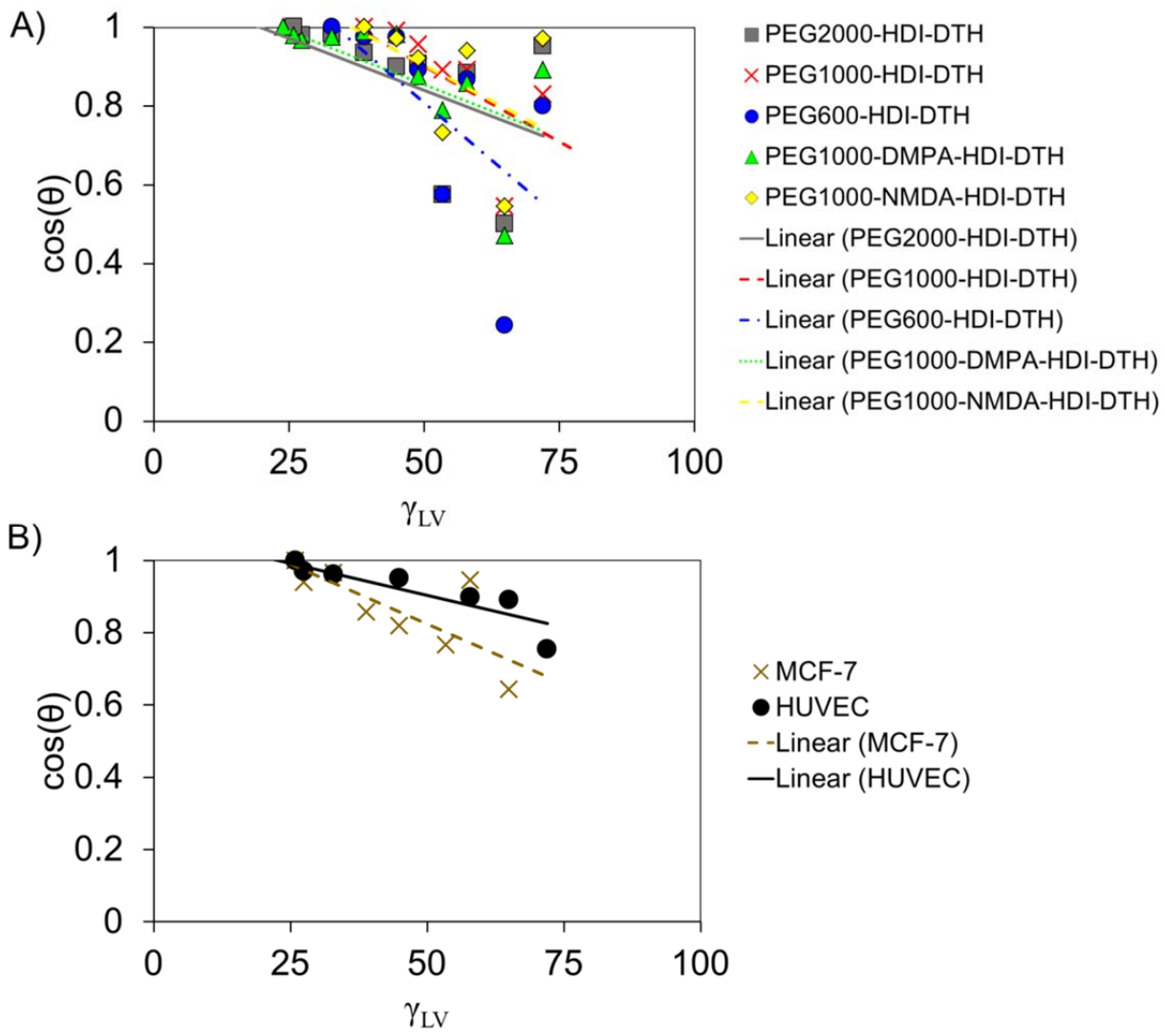

Figure S2: Zisman plots: A more negative slope designates a more apolar surface: A.) Zisman plots of PU microgel particles B.) Zisman plots of cell monolayers

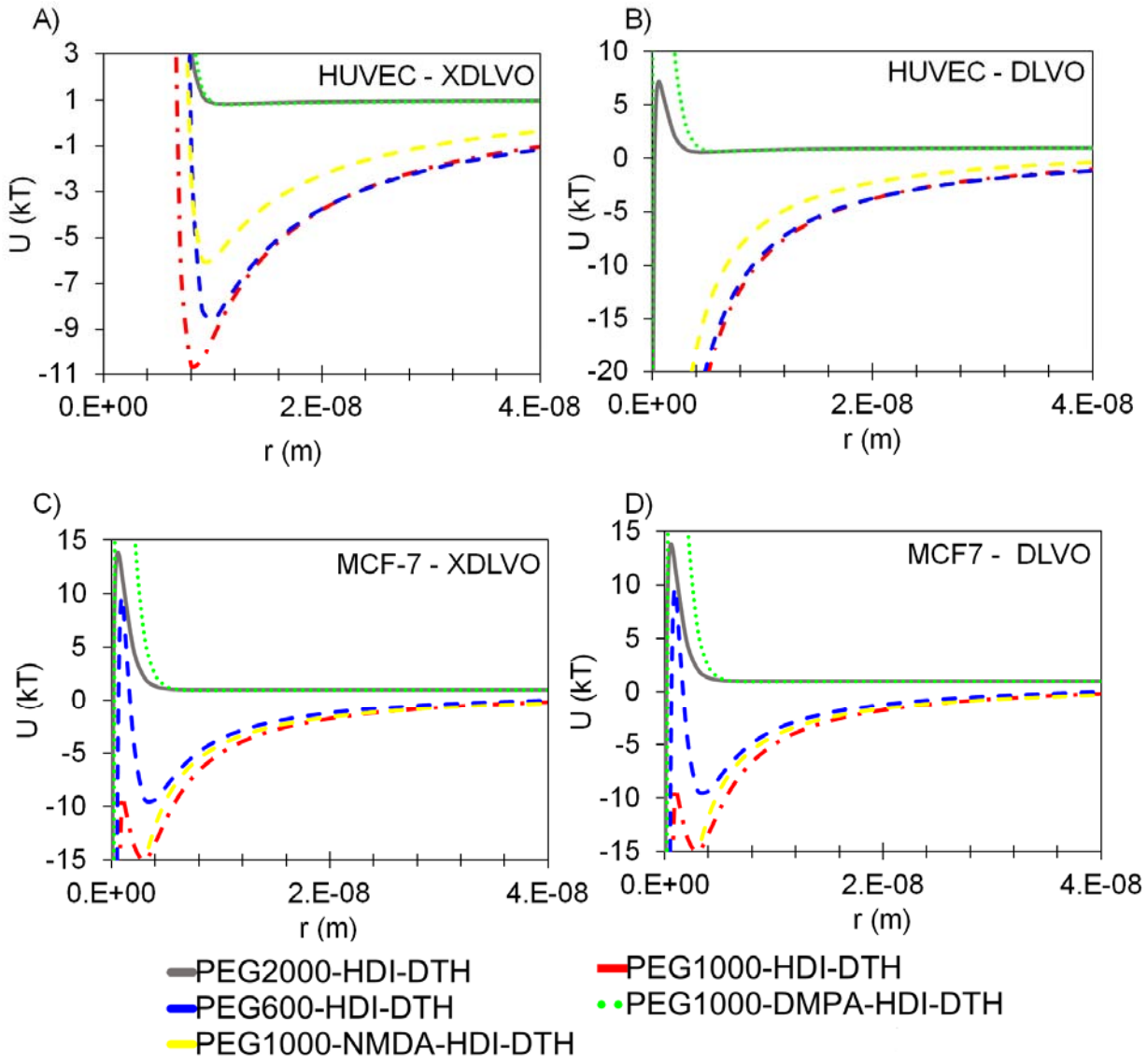

Figure S3: Dehydrated Interactions between Cells and Microgel Particles: Interactions are calculated with no solvent phase intervening between cells and particles. A.) HUVEC XDLVO interactions B.) HUVEC DLVO interactions C.) MCF-7 XDVLO Interactions D.) MCF-7 DLVO interactions

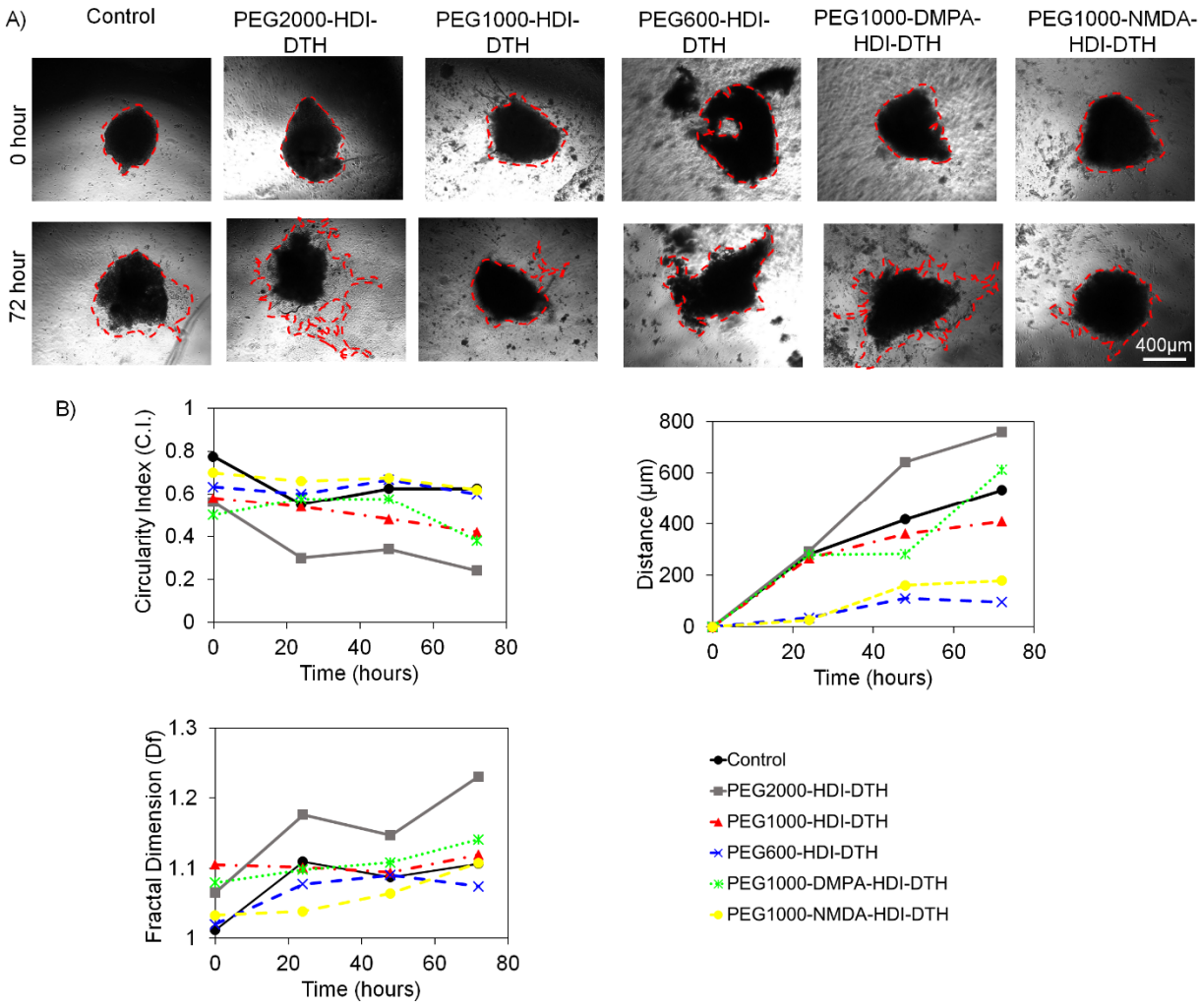

Figure S4: HUVEC-collagen I: Time dependent bright field images and changes in C.I. and D_f value and migration distance over 72 hours of microtissues embedded in ECM phase. A.) Time dependent bright field images of microtissue spreading with manually drawn contours B.) Morphometric changes with time of microtissue spreading

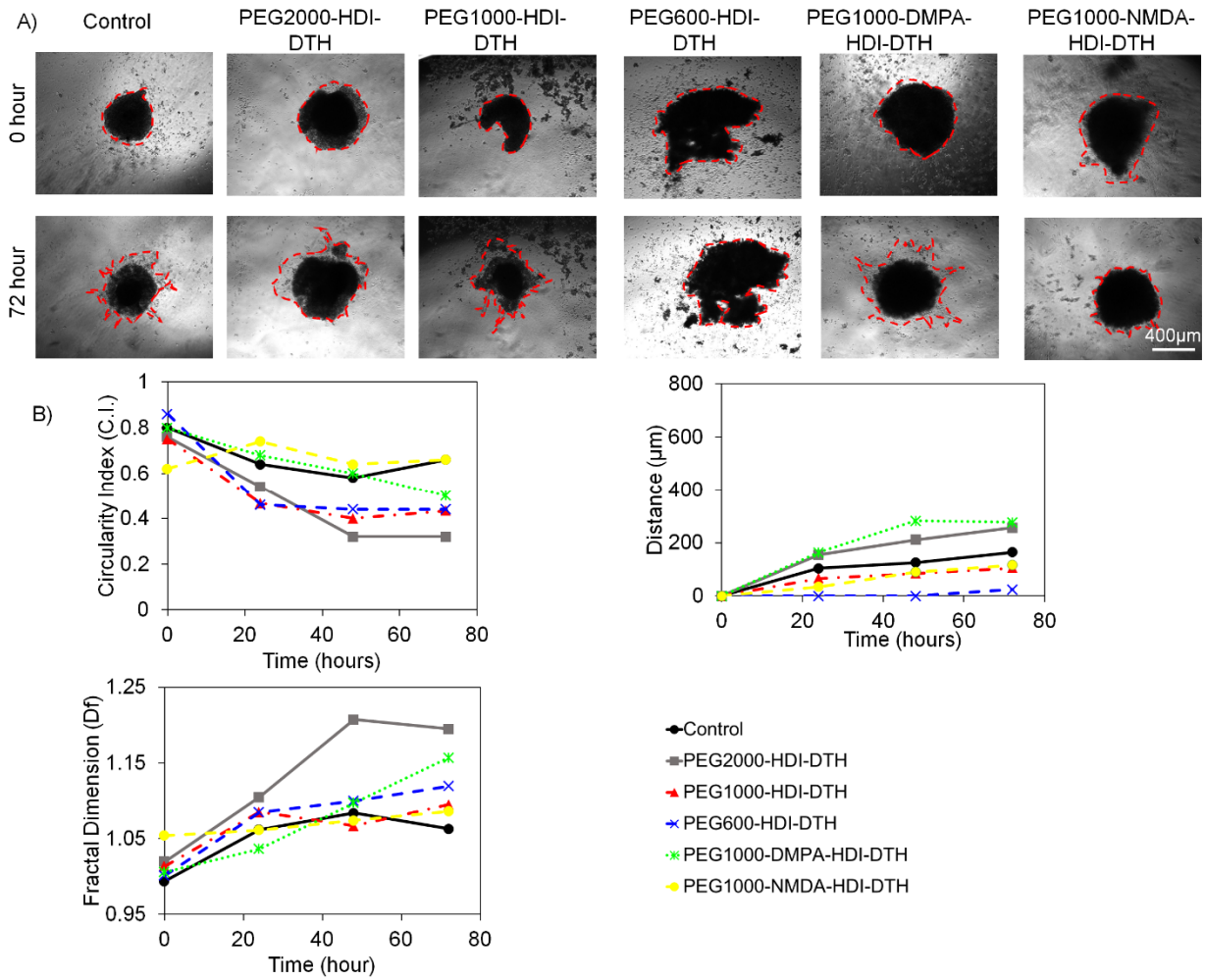

Figure S5: HUVEC-Matrigel®: Time dependent bright field images and changes in C.I. and D_f value and migration distance over 72 hours of microtissue embedded in ECM phase. A.) Time dependent bright field images of microtissue spreading with manually drawn contours B.) Morphometric changes with time of microtissue spreading

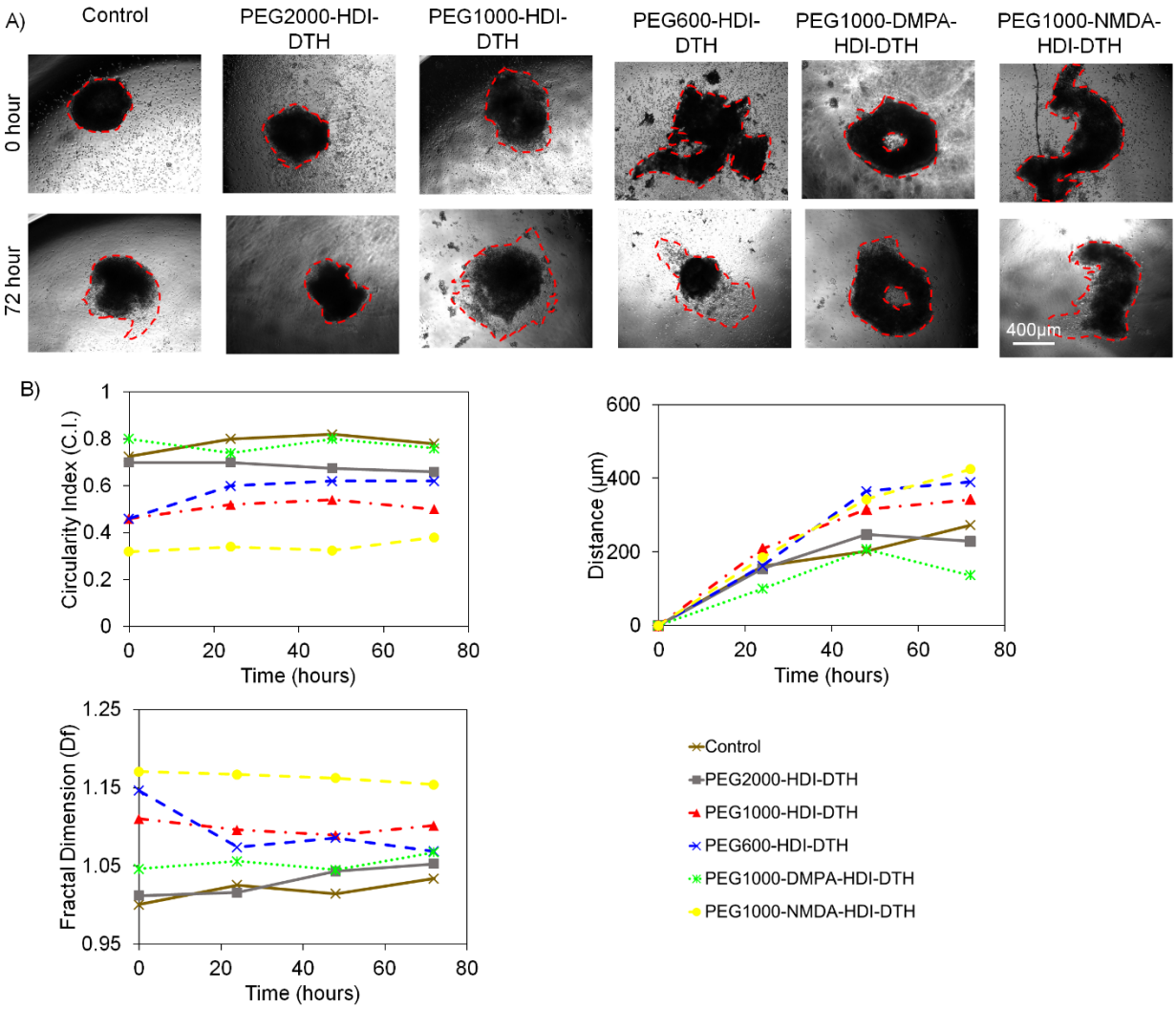

Figure S6: MCF7-collagen I: Time dependent bright field images and changes in C.I. and D_f value and migration distance over 72 hours of microtissue embedded in ECM phase. A.) Time dependent bright field images of microtissue spreading with manually drawn contours B.) Morphometric changes with time of microtissue spreading

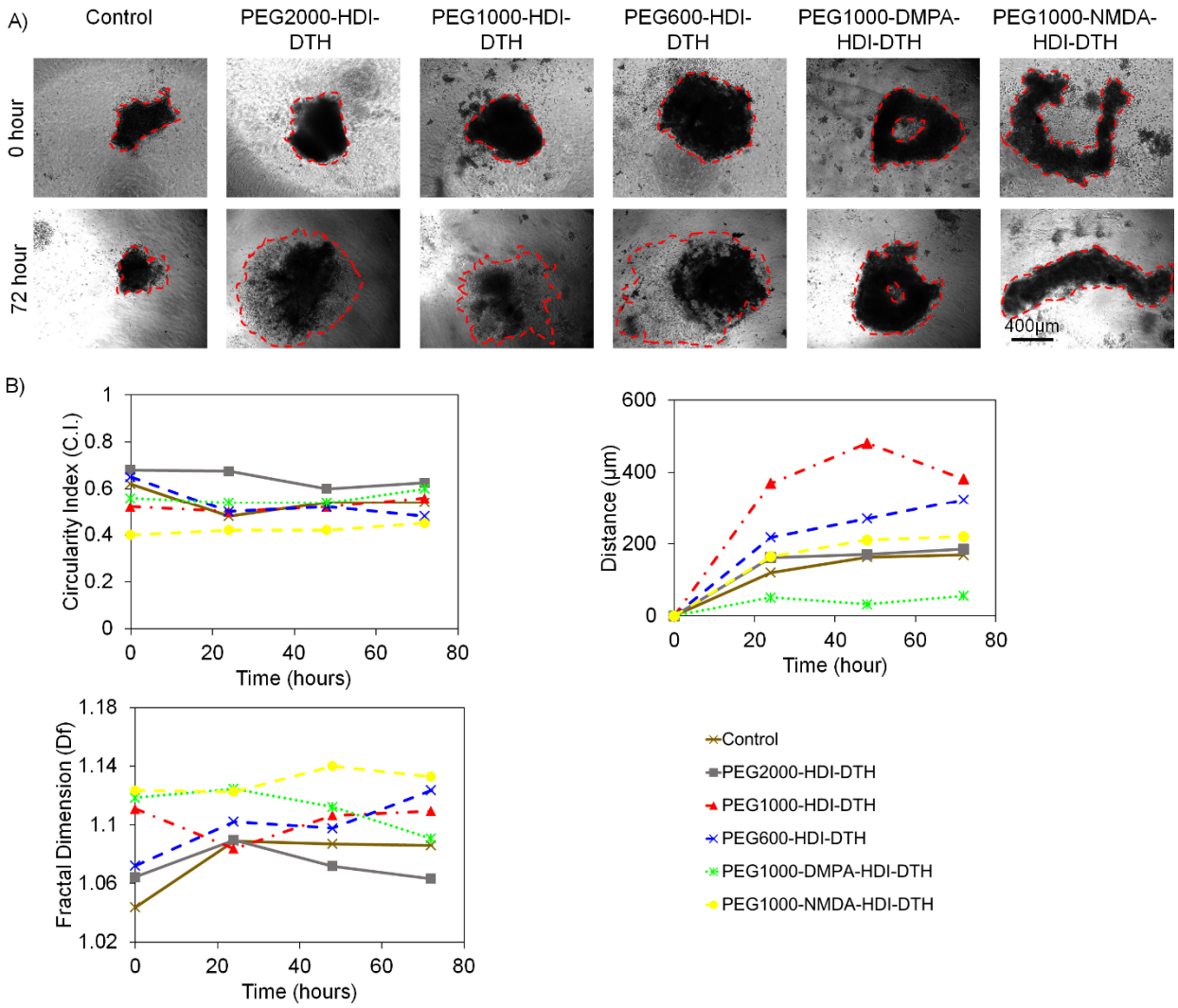

Figure S7: MCF7-Matrigel®: Time dependent bright field images and changes in C.I. and D_f value and migration distance over 72 hours. A.) Time dependent bright field images of microtissue spreading with manually drawn contours B.) Morphometric changes with time of microtissue spreading

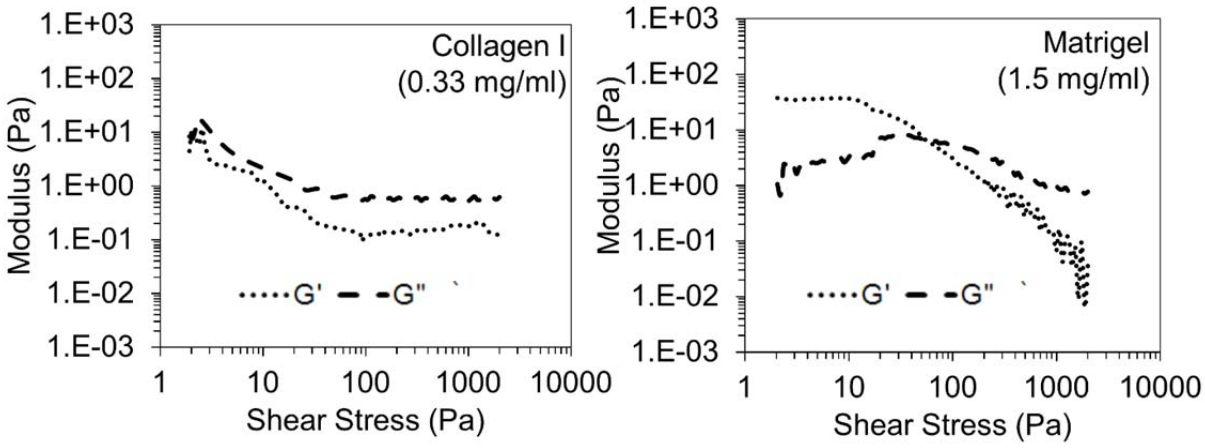

Figure S8: Rheology of ECM phases: Amplitude sweeps of Collagen I and Matrigel® at 1 Hz

Supplementary Tables S1-S9:

Table S1: Surface Tension Components of diagnostic liquids (dynes/cm)

Liquid	γ_l Surface Tension	γ^d Apolar-Dispersive	γ^p Polar	γ^+ Lewis Acid	γ^- Lewis Base
Water	72.8	21.8	51.0	25.0	25.0
Glycerol	64.0	34.0	30.0	3.92	57.4
Formamide	58.0	39.0	19.0	2.28	39.6
Thiodiglycol	53.5	38.1	15.4	n/a	n/a
Methylene iodide	49.0	44.9	4.10	n/a	n/a
n-Bromo naphthalene	45.0	45.0	0.00	0.00	0.00
1-Methylnaphthalene	39.3	25.8	13.5	0.00	0.00
Dicyclohexyl	32.7	32.7	0.00	0.00	0.00
n-Hexadecane	27.6	27.6	0.00	0.00	0.00
n-Tridecane	26	26	0.00	0.00	0.00
n-Decane	24	24	0.00	0.00	0.00

Values taken from [5, 6]

Table S2: Viability of Microtissues

Colloid	HUVEC absorbance	MCF-7 absorbance
Control	397 +/-28	398+/- 52
PEG2000-HDI-DTH	409 +/- 20	471+/- 67
PEG1000-HDI-DTH	414 +/- 89	454+/- 31
PEG600-HDI-DTH	447 +/- 42	626+/-123
PEG1000-DMPA-HDI-DTH	416+/- 4	535+/-126
PEG1000-NMDA-HDI-DTH	444+/-25	430+/- 73

Microtissue viability at 48 hours post-formation using alamar blue studies

Table S3: Contact angle on cell monolayers

Liquid	HUVEC	Fixed HUVEC	MCF-7	Fixed MCF-7
Water	0	15	20	16
Glycerol	49	41	36	50
Formamide	19	27	19	19
Thiodiglycol	36	26	38	40
Methylene Iodide	48	47	53	54
1-Bromonaphthalene	34	38	38	35
1-Methylnaphthalene	29	18	37	31
Dicyclohexyl	12	0	20	15
n-Hexadecane	20	16	25	20
n-Tridecane	13	14	0	0
n-Decane	0	0	0	0

Both glutaraldehyde fixed and non-fixed cell monolayers were measured

Table S4: Contact angle on PU colloids

Liquid	PEG2000-HDI-DTH	PEG1000-HDI-DTH	PEG600-HDI-DTH	PEG1000-DMPA-HDI-DTH	PEG1000-NDMA-HDI-DTH
Water	18	34	37	27	14
Glycerol	60	57	76	62	57
Formamide	28	27	30	31	20
Thiodiglycol	55	27	55	38	43
Methylene Iodide	25	17	27	29	23
1-Bromonaphthalene	26	8	13	11	14
1-Methylnaphthalene	21	0	13	9	0
Dicyclohexyl	11	0	0	13	0
n-Hexadecane	12	0	0	15	0
n-Tridecane	0	0	0	12	0
n-Decane	0	0	0	0	0

Polymers are solvent cast from 1% DMSO solutions onto acid washed glass coverslips

Table S5: Theoretical surface energy of PU colloids according to various theories (dyne/cm)

Substratum	Zisman	VOGCT			
	γ_c CST	γ_1^{LW} Van der Waals	γ_1^+ Lewis acid	γ_1^- Lewis base	γ_{s1} Surface energy
PEG2000-HDI-DTH	26.0	40.6	0.00	83.3	40.6
PEG1000-HDI-DTH	40.8	44.6	0.00	58.0	44.6
PEG600-HDI-DTH	35.8	43.9	0.00	82.1	43.9
PEG1000-NMDA-HDI-DTH	38.0	43.7	0.00	81.2	43.7
PEG1000-DMPA-HDI-DTH	24.8	44.2	0.00	74.9	44.2
HUVEC	24.0	37.6	0.00	76.7	37.6
Fixed HUVEC	22.0	36.0	2.29	50.6	57.5
MCF-7	26.0	36.0	1.23	53.7	52.2
Fixed MCF-7	26.0	37.2	0.00	71.7	37.7
Agar	24.6	31.3	4.89	47.6	61.8
Collagen Type 1	36.5	42.1	0.44	18.2	47.7
Matrigel	33.7	38.4	0.16	40.4	43.4

Subscript 1 denotes the water/glycerol combination for vOGCT calculations. Negative square roots obtained in solution of EQ. 7 were interpreted as zero.

Table S6: Theoretical surface energy of PU colloids according to various theories (dyne/cm)

Substratum	VOGCT			
	γ_2^{LW} Van der Waals	γ_2^+ Lewis Acid	γ_2^- Lewis Base	γ_{s2} Surface Energy
PEG2000-HDI-DTH	40.6	.27	58.6	48.5
PEG1000-HDI-DTH	44.6	0.29	41.9	51.5
PEG600-HDI-DTH	43.9	0.26	40.1	50.3
PEG1000-NMDA-HDI-DTH	43.7	0.33	56.5	52.4
PEG1000-DMPA-HDI-DTH	44.2	0.05	52.8	47.4
HUVEC	37.6	1.05	59.6	53.5
Fixed HUVEC	36.0	0.83	59.5	50.0
MCF-7	36.0	1.70	50.9	54.5
Fixed MCF-7	37.2	1.32	54.0	54.1
Agar	31.3	2.92	54.8	56.6
Collagen Type 1	42.1	0.00	25.7	42.1
Matrigel	38.4	1.30	31.4	51.2

Subscript 2 denotes the water/formamide combination for vOGCT calculations

Table S7: Rheological properties of microtissues

PU Microgel Particle	MCF-7 microtissue G′ (Pa)	HUVEC Microtissue G′ (Pa)	MCF-7 microtissue G′/G″	HUVEC Microtissue G′/G″
Control	0.5	0.6	0.4	0.0
PEG2000-HDI-DTH	3.3	65	2.3	2.7
PEG1000-HDI-DTH	2.4	4.0	0.0	1.5
PEG600-HDI-DTH	3590	2930	3.0	3.8
PEG1000-DMPA-HDI-DTH	1.4	2.8	2.0	2.0
PEG1000-NDMA-HDI-DTH	1.4	0.9	1.5	2.3

G′ and G″ are taken from the linear region of amplitude sweeps in figure 4

Table S8: Contact energies of particles with cells and ECM phases

PU	$J_{Particle-Particle}$	$J_{Particle-Medium}$	$J_{Particle-HUVEC}$	$J_{Particle-MCF-7}$	Volume	λ
PEG2000-HDI-DTH	2	2	5	2	2	10
PEG1000-HDI-DTH	-3	-4	-10	-14	8	70
PEG600-HDI-DTH	-4	-5	-6	-7	9	80
PEG1000-DMPA-HDI-DTH	3	3	3	3	3	20
PEG1000-NMDA-HDI-DTH	-1	-3	-3	0	7	60

Contact energies are taken from dehydrated interactions between cells and particles from figure S2. Interactions between particles and ECM phases is taken from figures 2 and 3

Table S9: Contact energy of cells with cells and ECM phase

Cell Type	$J_{Cell-Cell}$	$J_{Cell-Medium}$	Volume	λ
HUVEC	2	0	75	20
MCF-7	-3	-10	75	20

Contact energies of cells with one another and ECM phases is taken from figure 2 and figure 3

References

[1] R.M. Merks, S.V. Brodsky, M.S. Goligorksy, S.A. Newman, J.A. Glazier, Cell elongation is key to in silico replication of in vitro vasculogenesis and subsequent remodeling, Developmental biology, 289 (2006) 44-54.
[2] J.F. Li, J. Lowengrub, The effects of cell compressibility, motility and contact inhibition on the growth of tumor cell clusters using the Cellular Potts Model, Journal of theoretical biology, 343 (2014) 79-91.
[3] T. Abdulla, L. Luna-Zurita, J.L. de la Pompa, J.M. Schleich, R. Summers, Epithelial to mesenchymal transition-the roles of cell morphology, labile adhesion and junctional coupling, Computer methods and programs in biomedicine, 111 (2013) 435-446.
[4] N.J. Poplawski, U. Agero, J.S. Gens, M. Swat, J.A. Glazier, A.R. Anderson, Front instabilities and invasiveness of simulated avascular tumors, Bulletin of mathematical biology, 71 (2009) 1189-1227.
[5] E. Nyilas, W.A. Morton, R.D. Cumming, D.M. Lederman, T.H.B. Chiu, R. E., Effects of polymer surface molecular structure and force-field characteristics on blood interfacial phenomena, Journal of biomedical materials research, 11 (1977) 51-68.
[6] C.J. van Oss, Interfacial Forces in Aqueous Media, 2nd ed., Taylor & Francis, Boca Raton, FL, 2006.